

Solvothermal Synthesis of Lanthanide-doped NaYF₄ Upconversion Crystals with Size and Shape Control: Particle Properties and Growth Mechanism

Chunning Sun,^{*[a]} Michael Schäferling,^[b] Ute Resch-Genger,^[c] and Michael Gradzielski^{*[a]}

Abstract: Lanthanide-doped NaYF₄ upconversion nano- and microcrystals were synthesized via a facile solvothermal approach. Thereby, the influence of volume ratios of ethylene glycol (EG)/H₂O, molar ratios of NH₄F/RE³⁺ (RE³⁺ represents the total amount of Y³⁺ and rare-earth dopant ions), Gd³⁺ ion contents, types of activator dopant ions, and different organic co-solvents on the crystal phase, size, and morphology of the resulting particles were studied systematically. A possible formation mechanism for the growth of crystals of different morphology is discussed. Our results show that the transition from the α - to the β -phase mainly depends on the volume ratio of EG/H₂O and the molar ratio of NH₄F/RE³⁺,

while the morphology and size could be controlled by the type of organic co-solvent and Gd³⁺ dopant ions. Furthermore, the reaction time has to be long enough to convert α -NaYF₄ into β -NaYF₄ during the growth process to optimize the upconversion luminescence. The formation of larger β -NaYF₄ crystals, which possess a higher upconversion luminescence than smaller particles, proceeds via intermediates of smaller crystals of cubic structure. In summary, our synthetic approach presents a facile route to tailor the size, crystal phase, morphology, and luminescence features of upconversion materials.

1. Introduction

In the last years, lanthanide-doped upconversion (UC) materials have attracted ample interest because of their multitude of sharp emission bands originating from their ladder-like energy levels, long luminescence lifetimes in the microsecond region, high chemical stability, and relatively low toxicity.^[1] For appropriate dopant lanthanide ions, they can convert near-infrared (NIR) excitation light into visible or ultraviolet (UV) luminescence. Therefore, they are considered as promising luminescent carriers and reports for applications in photodynamic therapy and optogenetics,^[2] bioimaging,^[3] sensing,^[4] solar energy conversion,^[5] and other fields.^[6]

Lanthanide UC materials commonly consist of an optically transparent and chemically inert inorganic host of low phonon energy, sensitizer ions that have a relatively high absorption cross-section like Yb³⁺, and emissive activator ions such as Er³⁺, Tm³⁺, and Ho³⁺ ions. To date, rare-earth-based oxides,^[7]


oxysulfides,^[8] oxyfluorides,^[9] phosphates,^[10] vanadates^[11] and fluorides^[12] have been widely investigated as host matrices. For constructing UC materials, a proper host material is carefully chosen to have low lattice phonon energies, high transparency at the excitation and emission wavelength, and excellent chemical stability. Halides like chlorides, bromides, and iodides typically exhibit low phonon energies (< 300 cm⁻¹). Nonetheless, their hygroscopic nature inhibits their application. Oxides exhibit high chemical stability, while their phonon energies are generally larger than 500 cm⁻¹, which can favor nonradiative deactivation of the excited energy levels of the sensitizer and activator ions. In contrast, fluorides usually exhibit relatively low phonon energies (~350 cm⁻¹) and high chemical stability. Therefore, fluorides, like NaYF₄, are the most frequently used host materials.^[13] To minimize energy loss processes due to cross-relaxation, typically a relatively high amount of the sensitizer, commonly Yb³⁺ with its simple two energy-level structure in a concentration of about 20 mol%, and a relatively low amount of the activator, normally less than 2 mol%, are used.


For the synthesis of UC nano- and microcrystals, several synthetic approaches have been used, including the thermal decomposition method,^[14] hydro/solvothermal method,^[15] and coprecipitation method.^[16] The hydro/solvothermal synthesis utilizes a solvent under high pressures and mild temperatures to speed up reactions between solids. This presents an effective and convenient process in preparing various inorganic materials with diverse controllable morphologies and architectures in terms of cost and potential for large-scale production. Li's group^[17] developed a liquid-solid-solution (LSS) strategy to prepare UC nanocrystals via the solvothermal method using oleic acid as a stabilizer. Well-defined UC crystals with tunable size can also be prepared via the LSS method by changing

[a] C. Sun, Prof. Dr. M. Gradzielski
Stranski-Laboratorium für Physikalische und Theoretische Chemie, Institut für Chemie, Technische Universität Berlin, 10623 Berlin (Germany)
E-mail: sunchunning@gmail.com
michael.gradzielski@tu-berlin.de

[b] Prof. Dr. M. Schäferling
Department of Chemical Engineering, Münster University of Applied Sciences, 48565 Steinfurt (Germany)

[c] Dr. U. Resch-Genger
Division Biophotonics (BAM-1.2), Federal Institute for Materials Research and Testing (BAM)

 Supporting information for this article is available on the WWW under <https://doi.org/10.1002/cnma.202000564>

 © 2020 The Authors. ChemNanoMat published by Wiley-VCH GmbH. This is an open access article under the terms of the Creative Commons Attribution License, which permits use, distribution and reproduction in any medium, provided the original work is properly cited.

experimental parameters, like ligand amount, F^- concentration, and impurity doping.^[13a,18] Since these UC crystals are hydrophobic, post-modification is often particularly for all applications involving the aqueous environment.^[4f] To circumvent post-synthetic surface modifications, the synthesis of UC particles via the hydro/solvothermal method has been done by employing hydrophilic polymers or small molecules as ligands instead of the commonly used hydrophobic ones. For example, Zhang's group^[19] developed a simple solvothermal method to prepare polyethyleneimine (PEI)-capped UC nanoparticles with an average size of 50 nm. Also, polyvinylpyrrolidone (PVP) can be applied as well to synthesize hydrophilic UC nanoparticles.^[20] Lin's group^[21] used trisodium citrate (TSC) as the chelating agent, studied several factors, like the amount of ligand, reaction temperature, pH value, and fluoride source, for tailoring the crystal phases, shapes, and sizes of the resulting UC crystals. Moreover, Yang's group^[22] studied different surfactants (PVP, disodium ethylenediaminetetraacetate (EDTA), sodium dodecyl sulfate, and disodium tartrate) to control the crystal size and morphology. Zhao's group^[23] used different binary acids to prepare carboxyl-functionalized UC phosphors with controlled phase, shape, and size via a one-step hydrothermal method. These hydrophilic ligands apparently coordinate the metal ions to adjust the concentration of free ions, thereby affecting the growth kinetics of the particles. Additionally, the ligands can selectively adsorb on different facets of the crystallites, which could modulate the morphology and size of the crystals.

In this work, we describe the synthesis of hydrophilic lanthanide-doped $NaYF_4$ crystals with controllable size and morphology via the solvothermal method using disodium nitrilotriacetate (DSNTA) as the ligand and their subsequent characterization with respect to structure and optical performance. Nitrilotriacetic acid (NTA) and its salts are useful chelating agents, as they coordinate strongly with many metal ions, such as Fe, Co, and Ni,^[24] which can be ascribed to their versatility with respect to coordination modes (tetradentate ligand: three carboxyl groups and one nitrogen). However, the synthesis of UC crystals with the help of these ligands hasn't been investigated yet and accordingly was one of the aspects of this work. By systematically studying different reaction parameters, we could identify the volume ratio of ethylene glycol (EG) and water and the content of NH_4F as essential parameters for the control of the crystalline phase. As shown before, trivalent gadolinium ion (Gd^{3+}) can influence nucleation and growth processes of $NaYF_4$ nanocrystals, realizing simultaneous control over the size, crystal phase, and optical properties of the resulting nanocrystals.^[18] Accordingly, Gd^{3+} was used as the dopant to control the particle size in the solvothermal preparation process. The various dopant concentration of Gd^{3+} ion, different organic co-solvents, and the reaction time have profound effects on the control of crystalline morphology and size, which have been investigated in detail. Compared to the UC crystals prepared via the hydro/solvothermal method by other groups,^[15a,19–21,23] our results show that UC crystals with different sizes (from the nanoscale to microscale) and morphologies (sphere, prism, and rod-like shape) can be easily obtained

by simply changing the above-mentioned parameters (Table 1). Based on our findings, a feasible mechanism of morphological evolution and crystal growth is proposed. Additionally, the photoluminescence properties of the crystals were studied for particles differing in crystal phase, size, and chemical composition.

2. Results and Discussion

The aim of this work was to systematically establish correlations between the reaction conditions and the structure of UC crystals synthesized by a solvothermal method using hydrophilic DSNTA as coordinating ligand and to relate these features to their UCL. Synthesis parameters like the volume ratio of EG/ H_2O , the molar ratio of NH_4F/RE^{3+} , the organic co-solvents used, and the reaction time will influence phase structure, morphology, and size of lanthanide-doped $NaYF_4$ crystals, and thereby also the optical properties of the products. The effect of the type of activator dopant ion, the volume ratio of EG/ H_2O , the molar ratio of NH_4F/RE^{3+} , the Gd^{3+} ion content, and the type of organic co-solvent on the crystal phase, structure, morphology, size, and optical performance of UC materials were then investigated in detail. The synthetic process and resulting crystals obtained with different parameters are shown in Scheme 1.

2.1. Controlled synthesis of lanthanide-doped $NaYF_4$ crystals

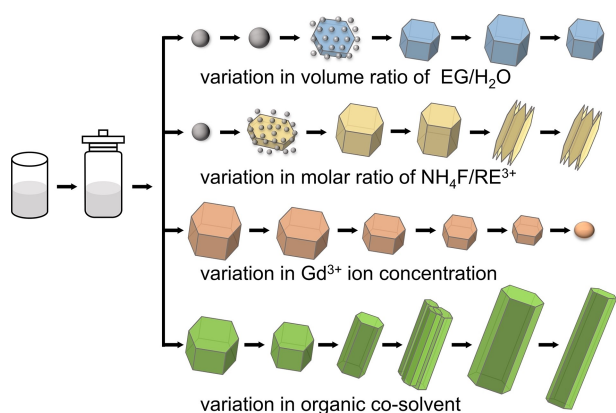
Synthetic conditions were investigated systematically to determine how these parameters affect the microscopic crystallinity as well as the mesoscopic/colloidal structure of the formed nano- and microcrystals.

2.1.1. Structure and morphology of the initial system

The crystal phase type and the phase purity of the samples with different activator dopant ions were firstly examined by XRD. The XRD patterns of the as-obtained $NaYF_4:Yb/Ln$ ($Ln = Er, Ho,$

Table 1. Comparison of various UC crystals obtained by the hydro/solvothermal method for different reaction conditions.

Ligand	Reaction Temperature	Size	Morphology	Ref.
citric acid	180 °C	microscale	sphere, prism, and octahedral	15a
PEI	200 °C	nanoscale	sphere	19
PVP	160 °C	nanoscale	quasi-sphere	20
TSC	180 & 220 °C	microscale	prism, rod, and irregular	21a–c
EDTA & TSC	180 °C	microscale	prism, disk and rod	21d
malonic acid	200 °C	microscale	prism, rod, and disk	23
DSNTA	190 °C	nanoscale & microscale	sphere, prism, rod, and irregular	this work



Scheme 1. Schematic illustration for the parameters on the final UC crystals.

or Tm) particles are shown in Figure 1a. All samples show peaks of a pure crystalline hexagonal β - NaYF_4 , which are in good accordance with the standard XRD pattern of hexagonal NaYF_4 (JCPDS No. 28-1192). No second phase is observed in the XRD patterns, implying that the crystalline phase is not affected by substituting Y^{3+} ions for Er^{3+} , Ho^{3+} , or Tm^{3+} ions, owing to the approximately equal radii of these lanthanide ions. As an example of Er^{3+} ion doping, Figure 1b shows the EDS pattern of the crystals, which reveals the presence of Na, Y, Yb, F and a small amount of Er element. It confirms the successful synthesis of $\text{NaYF}_4:\text{Yb}/\text{Er}$ crystals. Moreover, EDS mappings indicate that these component atoms were homogeneously distributed in the crystals (Figure 1h–l).

As can be seen from SEM and TEM images of β - $\text{NaYF}_4:\text{Yb}/\text{Er}$ (Figure 1c and d), the as-prepared sample contains fairly

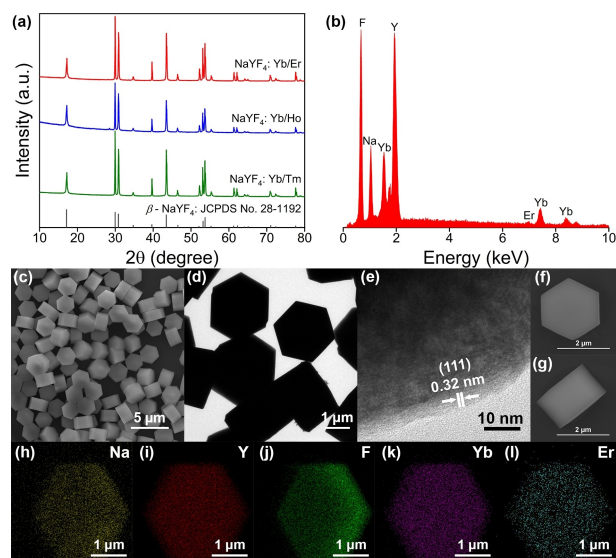


Figure 1. (a) XRD patterns of $\text{NaYF}_4:\text{Yb}/\text{Ln}$ and the standard data of hexagonal NaYF_4 (JCPDS No. 28-1192). (b) EDS analysis of $\text{NaYF}_4:\text{Yb}/\text{Er}$ microprisms. SEM (c), TEM (d) and HR-TEM (e) images of $\text{NaYF}_4:\text{Yb}/\text{Er}$ microcrystals. Top (f) and side (g) SEM images of $\text{NaYF}_4:\text{Yb}/\text{Er}$ microcrystals. EDS elemental mapping for (h) Na, (i) Y, (j) F, (k) Yb, and (l) Er of a single $\text{NaYF}_4:\text{Yb}/\text{Er}$ microparticle.

uniform hexagonal microprisms with excellent monodispersity and clear-cut crystallographic facets. The microprisms possess an average diameter of about $2.54\ \mu\text{m}$ and a length of about $1.50\ \mu\text{m}$ (aspect ratio of 0.59). The lattice fringes on the individual crystal are clearly distinguished in the HR-TEM image (Figure 1d), indicating the high crystallinity of the prepared microcrystals. The distance between the lattice fringes is measured to be about $0.32\ \text{nm}$, corresponding to the d-spacing for the (111) lattice planes of the hexagonal NaYF_4 structure. In addition, the higher magnification SEM images (Figure 1f and g) present ultra-smooth planes at both top and side surfaces without apparent defects and small particles attached on them. The average diameter and length change very little when Ho^{3+} or Tm^{3+} ions take the place of the Er^{3+} ion as the dopant ion (Figure S1). From the SEM images and the sharpness of the diffraction peaks in XRD patterns, it can be concluded that highly crystalline microprisms can be synthesized at a relatively low temperature, which is important for phosphors with fewer defect states and stronger luminescence. The general morphology and size of the as-obtained products are independent of activator dopant ions in β - NaYF_4 , as depicted in Table 2.

2.1.2. Effect of volume ratio of EG/H₂O

For the hydro/solvothermal method, the selected solvent can influence the solubility, diffusion, and reactivity of the reagents during the crystallization and particles with different morphology and size can be obtained. For instance, Song et al.^[25] showed that $\text{Gd}_2\text{O}_2\text{S}:\text{Eu}$ spheres with tunable size were synthesized by adjusting the volume ratio of EG/ethanol to change the diffusion rate of ions in the solution. Therefore, the choice of the solvent should be important and for that reason, we investigated systematically the solvent mixture of EG and H_2O .

For that purpose, $\text{NaYF}_4:\text{Yb}/\text{Er}$ samples were prepared by applying the same procedure, but varying the volume ratios of EG/ H_2O . The XRD patterns of particles obtained with different EG/ H_2O volume ratios, as well as the respective standard data of cubic and hexagonal NaYF_4 are shown in Figure S2 (Supporting Information). Apparently, if the volume ratio of EG/ H_2O is lower than 1/3, the diffraction patterns of the obtained crystals match well with the corresponding standard data of cubic NaYF_4 (JCPDS No. 06-0342). For a volume ratio of EG/ H_2O of 1/2, in addition to the characteristic peaks of the cubic phase, further

Table 2. Summary of samples prepared with different activator dopant ions.

Dopant ions ^[a]	Morphology	Structure	Average diameter [μm]	Average length [μm]	Aspect ratio
Yb/Er	microprism	hexagonal	2.54	1.50	0.59
Yb/Ho	microprism	hexagonal	2.36	1.40	0.59
Yb/Tm	microprism	hexagonal	2.43	1.39	0.57

[a] other synthetic parameters: EG/ H_2O = 2/1, $\text{NH}_4\text{F}/\text{RECl}_3$ = 7/1, reaction time: 12 h.

peaks start to appear, which can be indexed to the hexagonal NaYF₄ (JCPDS No. 28-1192). This indicates that the final system consists of both cubic and hexagonal phases of NaYF₄. When the volume ratio EG/H₂O is increased further, the XRD results are consistent with the standard hexagonal NaYF₄ XRD patterns. No further peaks are observed, implying the formation of pure crystalline β-NaYF₄:Yb/Er in the obtained products.

Figure 2 shows representative SEM images of NaYF₄:Yb/Er crystals prepared by using solvents with different mixing ratios. At a low EG/H₂O volume ratio, the sample is made up of spherical nanoparticles with an average diameter of 102 nm (EG/H₂O = 1/4) and 121 nm (EG/H₂O = 1/3), respectively (Figure 2a and b). As the ratio of EG/H₂O increases to 1/2, microsheets with a mean diameter of about 4.43 μm are observed together with nanoparticles (Figure 2c), consisting with the XRD result of the sample. As the volume ratio increases to 1, microprisms with a diameter of 1.92 μm and length of 1.06 μm are obtained, while the nanoparticles disappear completely (Figure 2d). When the volume ratio of EG/H₂O rises to 2, the SEM image (Figure 2e) exhibits regular and uniform hexagonal-shaped morphology with a smooth surface, and the crystal size is 2.54 μm in diameter and 1.50 μm in height (aspect ratio of 0.59). Further increasing the volume ratio of EG/H₂O, the morphology remains unchanged, whereas the average diameter and height of prepared crystals tend to decrease (Figure 2f), the surface of the as-made crystals, however, appears to be coarser compared with those obtained under the

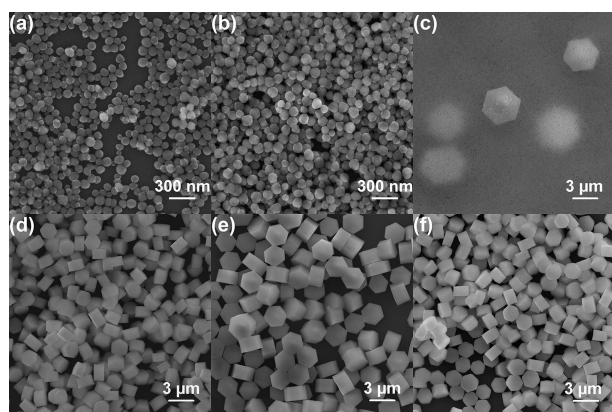


Figure 2. SEM images of NaYF₄:Yb/Er prepared at different volume ratios of EG/H₂O. (a) 1/4, (b) 1/3, (c) 1/2, (d) 1/1, (e) 2/1, (f) 3/1.

volume ratio of 2. The final morphologies and sizes of the as-synthesized crystals are summarized in Table 3.

These data confirm that the volume ratio of EG/H₂O plays a dominant role in controlling the morphology and crystallinity of the final crystals. For optimizing the content of hexagonal NaYF₄:Yb/Er and having a high degree of monodispersity, as well as well-defined crystallographic facets, the optimal volume ratio of EG/H₂O was found to be 2.

2.1.3. Effect of molar ratio of NH₄F/RE³⁺

Xu and co-workers^[26] have shown that the molar ratio of fluoride ion to lanthanide ions can strongly influence the final morphology of the product. Various morphologies of micro-sized NaYF₄:Yb/Er crystals could be controlled by simply adjusting the molar ratios between fluoride ion and lanthanide ions. This parameter affects the growth and morphology evolution during crystal formation.

To investigate the effect of the molar ratio of NH₄F/RE³⁺ on the structure and morphology of NaYF₄:Yb/Er crystals, a series of control experiments were carried out with various molar ratios of NH₄F/RE³⁺ while the other experimental parameters remained constant. The corresponding XRD patterns of the final products are shown in Figure S3. The samples prepared with different molar ratios of NH₄F/RE³⁺ exhibit quite different XRD patterns, the sample obtained at a low molar ratio (NH₄F/RE³⁺ = 4) is consistent with the standard data of cubic NaYF₄ (JCPDS No. 06-0342). As the molar ratio increases to 6, the characteristic peaks of the obtained XRD show the coexistence of the standard cubic and hexagonal phase of NaYF₄, implying that a new hexagonal phase appears in the final product. At the same time, the intensity of the peaks of the cubic phase decreases compared with those obtained at a low molar ratio. When the molar ratio is further increased (NH₄F/RE³⁺ > 7), the XRD patterns are in excellent agreement with the standard data of the hexagonal NaYF₄ phase (JCPDS No. 28-1192), no other impurity peaks are detected, indicating the presence of pure β-NaYF₄:Yb/Er.

Figure 3 shows typical SEM images of the samples prepared with different molar ratios of NH₄F/RE³⁺. As observed in Figure 3a, nanoparticles with a mean diameter of 83 nm are obtained at a lower molar ratio (NH₄F/RE³⁺ = 4), these nanoparticles are of cubic structure, as ascertained by the XRD analysis. When the experiment is conducted at NH₄F/RE³⁺ = 6,

Table 3. Summary of NaYF₄:Yb/Er crystals prepared with different volume ratios of EG/H₂O.

EG/H ₂ O ^[b]	Morphology	Structure	Average diameter [μm]	Average length [μm]	Aspect ratio
1/4	nanosphere	cubic	0.10	–	–
1/3	nanosphere	cubic	0.12	–	–
1/2	nanosphereµsheet	cubic&hexagonal	0.05&4.43	–	–
1/1	microprism	hexagonal	1.92	1.06	0.55
2/1	microprism	hexagonal	2.54	1.50	0.59
3/1	microprism	hexagonal	1.88	1.09	0.58

[b] other synthetic parameters: NH₄F/RECl₃ = 7/1, reaction time: 12 h.

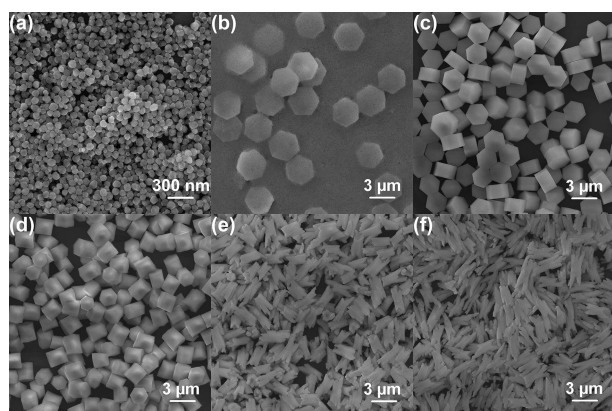


Figure 3. SEM images of NaYF₄:Yb/Er prepared at different molar ratios of NH₄F/RE³⁺. (a) 4, (b) 6, (c) 7, (d) 8, (e) 12, (f) 16.

the product is composed of nano-sized α -NaYF₄:Yb/Er spheres and micro-sized β -NaYF₄:Yb/Er sheets with an average diameter of 3.54 μ m (Figure 3b). As the molar ratio of NH₄F/RE³⁺ increases to 7, nanoparticles are no longer observed and only hexagonal microprisms with an average size of 2.54 μ m in diameter and 1.50 μ m in length are obtained (Figure 3c). With the molar ratio further increased to 8, the morphology is shown to be hexagonal as well (Figure 3d). The mean diameter of the crystals decreased to 1.93 μ m, while the mean length increased to 1.76 μ m, and the corresponding aspect ratio is slightly increased. For still higher molar ratio, irregularly structured hexagonal NaYF₄:Yb/Er crystals of increasing length are obtained (Figure 3e and f).

Apparently, the molar ratio of NH₄F/RE³⁺ has a significant influence on the structure and morphology of the resulting crystals. The optimal molar ratio of NH₄F/RE³⁺ is 7, which allows the formation of micro-sized β -NaYF₄:Yb/Er particles. The corresponding morphologies and sizes, as well as aspect ratios of the products are summarized in Table 4.

2.1.4. Effect of Gd³⁺ content

Liu and co-workers^[18] have shown that an increasing Gd³⁺ ion dopant concentration slows the diffusion of F⁻ ions to the surface, inducing a reduction of the NaYF₄ nanocrystal size by increasing the electron charge density on the surface of the

crystals. A similar result was also observed for a NaYbF₄ host matrix.^[27] In addition, different sizes of the dopant ions can be used to modify the electronic transfer conditions within the crystals. In this respect, Gd³⁺ is particularly interesting because of its paramagnetic properties.^[1b,28]

The effect of Gd³⁺ concentration on the structure and morphology of NaYF₄:Yb/Er crystals was studied by varying it. The crystallinity of as-prepared NaYF₄:Yb/Er/Gd (20/2/x mol%, x=0~60) crystals were firstly examined by XRD patterns (Figure S4). The products show well-defined peaks for a Gd³⁺ content in the range of 0% to 40%, confirming their good crystallinity, and the XRD patterns of these products coincide well with the standard hexagonal NaYF₄ pattern of JCPDS No. 28-1192. This indicates that a pure hexagonal phase structure of the lanthanide-doped NaYF₄ is formed when the Gd³⁺ dopant concentration is less than 40%. With increasing Gd³⁺ dopant concentrations, the relative intensities of the characteristic peaks are reduced compared to those obtained with lower Gd³⁺ content, as shown in Figure S4. Nevertheless, these characteristic peaks still agree well with the standard XRD pattern of hexagonal NaYF₄. As the Gd³⁺ ion content increases further, the diffraction peaks shown in the XRD patterns broaden, and no extra diffraction peaks were observed, implying the formation of a homogeneous Y–Gd solid solution, because of the small structural difference between the hexagonal phases of NaGdF₄ and NaYF₄. In addition, owing to the gradual replacement of Y³⁺ by larger Gd³⁺ ions in the host, the volume of the unit-cell expands, resulting in the slight shift of the peaks toward lower diffraction angles in the XRD patterns.

Figure 4 shows representative SEM images of the samples obtained with different Gd³⁺ concentrations under the same synthetic conditions. Figure 2e, and Figure 4a and b reveal an inverse relationship between the amount of Gd³⁺ and the resulting size of the crystals for a Gd³⁺ ion dopant content increasing from 0% to 20%, while the hexagonal structure remains unchanged. The average diameter and height dramatically decrease to 1.70 μ m and 0.87 μ m for a Gd³⁺ content of 10%, and is further reduced to 1.13 μ m and 0.52 μ m when this dopant content reaches 20%. At the same time, the aspect ratio presents a slightly descending trend, with a reduction from 0.59 to 0.46. When the dopant content varies in the range of 30% to 50%, as shown in Figure 4c–e, the diameter and height continuously decrease to nanoscale dimensions. The synthesized products are composed of uneven hexagonal prisms in

Table 4. Summary of NaYF₄:Yb/Er crystals prepared with different molar ratios of NH₄F/RE³⁺.

NH ₄ F/RE ³⁺ [c]	Morphology	Structure	Average diameter [μ m]	Average length [μ m]	Aspect ratio
4	nanosphere	cubic	0.08	–	–
6	nanosphereµsheet	cubic&hexagonal	0.04&3.54	–	–
7	microprism	hexagonal	2.54	1.50	0.59
8	microprism	hexagonal	1.93	1.76	0.91
12	irregular microrod	hexagonal	1.06	2.27	2.14
16	irregular microrod	hexagonal	1.02	3.12	3.06

[c] other synthetic parameters: EG/H₂O = 2/1, reaction time: 12 h.

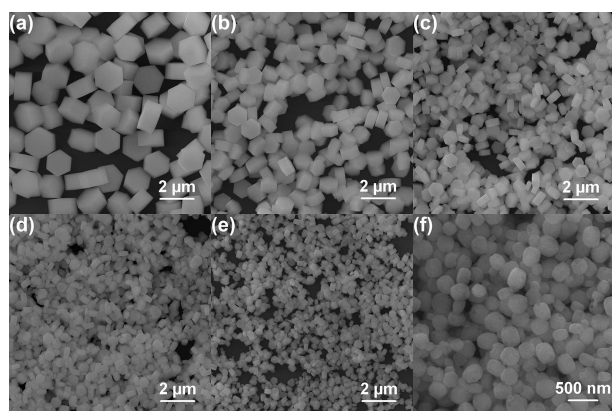


Figure 4. SEM images of products obtained with the different content of Gd^{3+} ion. (a) 10%, (b) 20%, (c) 30%, (d) 40%, (e) 50%, (f) 60%.

size and the crystal morphology of the obtained products is also hexagonal. Further increasing the Gd^{3+} content to 60% (Figure 4f) yields spherical nanoparticles with coarse surfaces instead of well-defined hexagonal prisms. The abovementioned XRD results of widening peaks confirm the reduction of the average crystal size with increasing Gd^{3+} content. It should be noted that the Gd^{3+} content not only leads to a reduction in particle size but also remarkably affects the crystal formation and growth. The structural information of the samples is summarized in Table 5.

2.1.5. Effect of different organic co-solvents

After having seen the importance of the organic co-solvent on the outcome of particle formation in 2.1.2, this effect was subsequently systematically assessed by substituting the low molecular weight organic solvent (EG) with higher molecular weight polyethylene glycols (PEGs) and propylene glycols (PPGs) in order to see whether this allows for further fine-tuning of the UC particles.

For that purpose, a series of experiments were conducted with various organic co-solvents substituting EG but otherwise retaining the reaction conditions. Figure S5 shows the XRD

patterns of the resulting crystals with the different organic co-solvents as well as standard data of the hexagonal $NaYF_4$ phase. The XRD results reveal that all crystals show conformity to the standard pattern of hexagonal $NaYF_4$ (JCPDS No. 28-1192).

Typical SEM images of the obtained particles are shown in Figure 5. The SEM images reveal that the crystals tend to grow into an irregular shape for PEG 200 and PEG 400 (Figure 5c and d). Apparently, well-defined crystals can only be obtained for low molecular weight molecules (Figure 5a and b). However, when PPGs are employed, uniform hexagonal microrods with excellent monodispersity and clear-cut crystallographic facets are formed. When the molecular weight of the PPG rises from 400 to 1000 g/mol, the mean diameter decreases from 2.85 μm to 1.67 μm , and the length is reduced from 6.32 μm to 3.03 μm . In addition, a reduction in aspect ratio takes place (Figure 5e and f). It is interesting to note that the methyl branching of the organic co-solvent apparently favors the formation of crystals with well-defined crystallographic facets, and this small modification in the chain of the second solvent component has a very large effect on the formed crystals. The corresponding features of the products are summarized in Table 6.

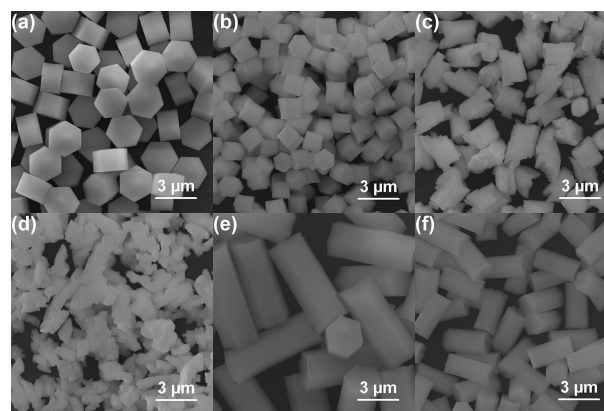


Figure 5. SEM images of products obtained with different organic co-solvents. (a) EG, (b) DEG, (c) PEG 200, (d) PEG 400, (e) PPG 400, (f) PPG 1000.

Table 5. Summary of $NaYF_4:Yb/Er/Gd$ crystals prepared with different Gd^{3+} dopant content.

Gd^{3+} content (mol%) ^[d]	Morphology	Structure	Average diameter [μm]	Average length [μm]	Aspect ratio
0	microprism	hexagonal	2.54	1.50	0.59
10%	microprism	hexagonal	1.70	0.87	0.51
20%	microprism	hexagonal	1.13	0.52	0.46
30%	nanoprism	hexagonal	0.72	0.31	0.43
40%	nanoprism	hexagonal	0.49	0.22	0.45
50%	nanoprism	hexagonal	0.32	0.18	0.56
60%	nanosphere	hexagonal	0.26	–	–

[d] other synthetic parameters: EG/ H_2O = 2/1, $NH_4F/RECl_3$ = 7/1, reaction time: 12 h.

Table 6. Summary of $NaYF_4:Yb/Er$ crystals prepared with different organic co-solvents.

Organic solvent ^[e]	Morphology	Structure	Average diameter [μm]	Average length [μm]	Aspect ratio
EG	microprism	hexagonal	2.54	1.50	0.59
DEG	microprism	hexagonal	1.45	1.22	0.84
PEG 200	irregular	hexagonal	1.50	2.36	1.57
PEG 400	irregular	hexagonal	–	3.38	–
PPG 400	microrod	hexagonal	2.85	6.32	2.22
PPG 1000	microrod	hexagonal	1.67	3.03	1.81

[e] other synthetic parameters: organic co-solvent/ H_2O = 2/1, $NH_4F/RECl_3$ = 7/1, reaction time: 12 h.

2.2. Crystal growth and formation mechanism

In order to obtain insights into the formation processes of the lanthanide-doped NaYF₄ crystals with different morphologies, β-NaYF₄:Yb/Er microprisms were used as a representative case to study the morphological evolution and crystal growth as a function of time by taking samples after different reaction times. This was done as they are also most interesting with respect to their optical properties revealed in the following section. Figure S6 presents XRD patterns of the crystallinity and phase transformation of NaYF₄:Yb/Er particles obtained after different reaction times. This shows a remarkable evolution with increasing reaction time. The diffraction peaks of the sample obtained after 2 h coincide with those of a pure cubic NaYF₄ phase (JCPDS No. 06-0342). As the time increases to 4 h, the XRD pattern shows additional peaks characteristic for the hexagonal phase of NaYF₄. This indicates that the initially present cubic crystals are converted into a hexagonal phase, which is then also present in the final product. Upon increasing the reaction time to 6 h and further to 12 h, the XRD patterns of the resulting particles are in excellent agreement with the standard data of the hexagonal NaYF₄ phase (JCPDS No. 28-1192), implying a complete disappearance of the cubic phase and one has now a pure hexagonal phase. Furthermore, the intensity of the diffraction peaks of the hexagonal phase increases as the reaction proceeds, revealing that the crystallinity is increasing with reaction time.

In parallel, the morphological evolution of the NaYF₄:Yb/Er particles was examined by SEM after different reaction times. The SEM images presented in Figure 6a–d show different particle morphologies as a function of reaction times. In the early stage, the DSNTA was introduced into the solution to form lanthanide-ligand complexes through coordination interaction. When the reaction temperature reaches 190 °C, the lanthanide ions can gradually be released as their binding in the complexes becomes weakened at high temperature and pressure. Then, Na⁺ and F⁻ ions react with RE³⁺ to generate small nuclei, these small nuclei grow into cubic NaYF₄:Yb/Er nanocrystals within a short time of ~2 h. Figure 6a shows that the sample prepared after 2 h consists of spherical nanoparticles with a mean diameter of 88 nm and the crystals formed are purely cubic (XRD analysis). The α-NaYF₄:Yb/Er nanoparticles then further serve as seeds for the growth of β-NaYF₄:Yb/Er as the reaction

proceeds. As shown in Figure 6b, when the reaction time increases to 4 h, a coexistence of hexagonal microprisms and spherical nanoparticles is observed, indicating the transition of nanoparticles into microprisms. As the reaction proceeds up to 6 h and further to 12 h (Figure 6c and d), the spherical nanoparticles have disappeared, and only microprisms with an average diameter of 2.54 μm and a height of 1.50 μm are present, implying the complete transformation from spherical α-NaYF₄:Yb/Er nanocrystals into β-NaYF₄:Yb/Er microprisms. Based on the above observations, the assumed formation mechanism of NaYF₄:Yb/Er microcrystals is illustrated in Figure 6e.

2.3. UC photoluminescence properties

Finally, we measured the UCL of the different UC particles under identical experimental settings. Relative changes of UCL emission were determined within four different measurement series (different volume ratios EG/H₂O, different Gd³⁺ co-dopant concentrations, different ratios of NH₄F/RE³⁺, and different organic co-solvents). Here it has to be kept in mind that for a comparison of UCL in absolute values different parameters have to be considered such as the influence of particle size and its effect on excitation power density, and the size dependent scattering behavior of UC particles.^[29] First, we investigated the UCL properties of NaYF₄ doped with Yb/Er, Yb/Ho, or Yb/Tm. The corresponding UCL spectra of β-NaYF₄:Yb/Ln are summarized in Figure 7a, showing the specific effect of the respective activator ions. The UCL spectrum of the β-NaYF₄:Yb/Er particles contains emissions bands centered at 524 nm, 544 nm, and 658 nm, which can be assigned to the ²H_{11/2}→⁴I_{15/2}, ⁴S_{3/2}→⁴I_{15/2} and ⁴F_{9/2}→⁴I_{15/2} transitions of Er³⁺, respectively.^[30] The spectrum of the β-NaYF₄:Yb/Ho sample exhibits an intense emission at 541 nm and a relatively weak emission centered at 645 nm originating from ⁵S₂→⁵I₈ and ⁵F₅→⁵I₈ transitions of Ho³⁺. In the case of the Yb/Tm doped particles, two strong emission bands at 475 nm (¹G₄→³H₆) and 800 nm (⁵F₅→⁵I₈), three weak emission bands at 450 nm (¹D₂→³F₄), 648 nm (¹G₄→³F₄), and 700 nm (³F₃→³H₆) are observed. In general, it can be stated that the photoluminescence properties are relatively similar for crystals doped with Er³⁺ ion and Ho³⁺ ion, while for Tm³⁺ ion, the primary signal appears at 800 nm.^[31]

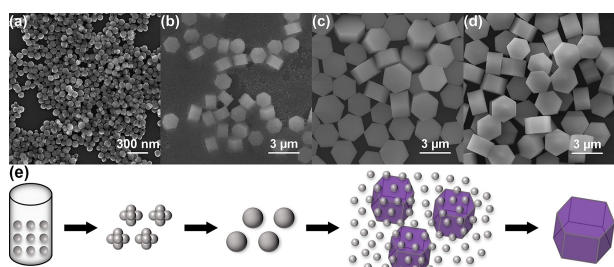


Figure 6. SEM images of products obtained after different times. (a) 2 h, (b) 4 h, (c) 6 h, (d) 12 h. (e) Possible formation mechanism of NaYF₄:Yb/Er crystals.

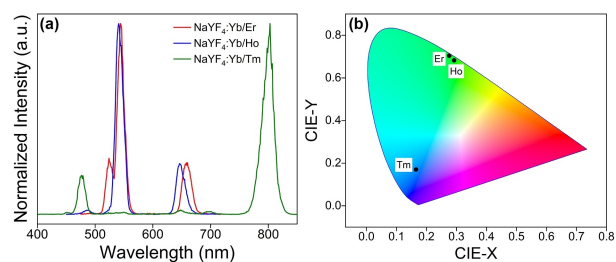


Figure 7. (a) Normalized UCL spectra and (b) CIE chromaticity diagram of NaYF₄:Yb/Ln under 976 nm excitation (molar ratio Yb/Ln of 20/2 mol%).

As to be expected, the luminescence features of the crystals, i.e., the emission bands, emission colors, and emission intensities are determined by the activator ions. In order to assess the emission color of the different UC particles, chromaticity coordinates of β -NaYF₄:Yb/Ln crystals were calculated according to the Commission Internationale de l'Éclairage (CIE) chromaticity diagram, based on the corresponding UCL under 976 nm excitation for the respective excitation power density used. The results are plotted in Figure 7b, which highlights the similarity of the Yb/Er and Yb/Ho doped particles, with the CIE color coordinates of β -NaYF₄:Yb/Er ($x=0.2754$, $y=0.7040$) and β -NaYF₄:Yb/Ho ($x=0.2920$, $y=0.6828$) being located in the green region, while the Yb/Tm system has a very different color output with β -NaYF₄:Yb/Tm ($x=0.1651$, $y=0.1707$) being located in the blue region.

Subsequently, we focused on Er³⁺ based systems and studied the effect of different synthetic parameters previously described in 2.1.2–2.1.5 on the UCL of the resulting particles. It should be noted that this comparison was done for screening purposes, i.e., to screen the influence of the different synthetic conditions used on the optical properties of the UC particles and not for really quantifying these effects, as for that different particle sizes and related surface quenching effects the actual excitation power density would have to be considered.^[29]

The obtained results are summarized in Figure 8. As can be seen from Figure 8a–d, the α -NaYF₄:Yb/Er crystals, formed at a low EG/H₂O volume ratio and NH₄F/RE³⁺ molar ratio, are barely emissive at the respective excitation power density used here as previously described in the literature.^[32] More pronounced green (544 nm) and red (658 nm) emissions appear as soon as β -NaYF₄:Yb/Er particles are present and become dominant. Based on the UCL spectra obtained for closely matching excitation conditions, it can be concluded that the intense UCL achieved by the formation of well-defined crystals with a hexagonal β -NaYF₄ structure is in good agreement with previous studies.^[33] The strongest emission is observed for an EG/H₂O volume ratio of 2/1, which is tentatively attributed to the well-defined crystallographic facets (Figure 2e).

The red-to-green ratio (R/G) of emission intensity is utilized to explain the luminescence changes of UC crystals prepared with various parameters, which is depicted in Figure 8e. The R/G value decreases from 1.04 to 0.30 for an increasing EG/H₂O volume ratio from 1/4 to 2/1. The R/G value remains at about 0.30 for UC crystals prepared with a NH₄F/RE³⁺ molar ratio above 6, except for the ones obtained at a low NH₄F/RE³⁺ molar ratio. A similar trend is observed for UC crystals obtained in a low molecular weight of organic co-solvent, while a significant increase in the R/G value occurs when PPG1000 is used as the co-solvent. In addition, it is evident that R/G value is sensitive to the concentration of Gd³⁺ and increases with increasing Gd³⁺ concentration. The difference in the R/G ratios of NaYF₄:Yb/Er/Gd may be attributed to a loss of crystallinity and a reduction in crystal size (see Figures 4 and S3). Moreover, it is worth mentioning that the tunable emission color of UC samples can be obtained by varying synthetic parameters, as evidenced in Figure S7.

3. Conclusion

In summary, lanthanide-doped NaYF₄ nano- and micro-sized upconversion crystals with different morphologies were successfully prepared via the solvothermal method using disodium nitrilotriacetate as the capping agent. The influence of the volume ratio of EG/H₂O, the molar ratio of NH₄F/RE³⁺, the Gd³⁺ ion dopant concentration, the type of activator dopant ions, different organic co-solvents was systematically studied. With the aid of this synthetic approach, the size, shape, and morphology of the resulting crystals can be tuned from spherical nanoparticles over nano/microprisms to microrods with high uniformity and monodispersity by carefully adjusting the synthesis parameters, showing a feasible route for controllable synthesis of upconversion crystals when compared to other studies.^[19–21]

The crystal phase transition from cubic to hexagonal phase mainly depends on the volume ratio of EG/H₂O and the molar ratio of NH₄F/RE³⁺, while the morphology is readily tuned by the choice of the organic co-solvents. Furthermore, the reaction time has to be long enough as apparently in the beginning always cubic α -NaYF₄ is formed, which under appropriate conditions then is converted into hexagonal β -NaYF₄ during the

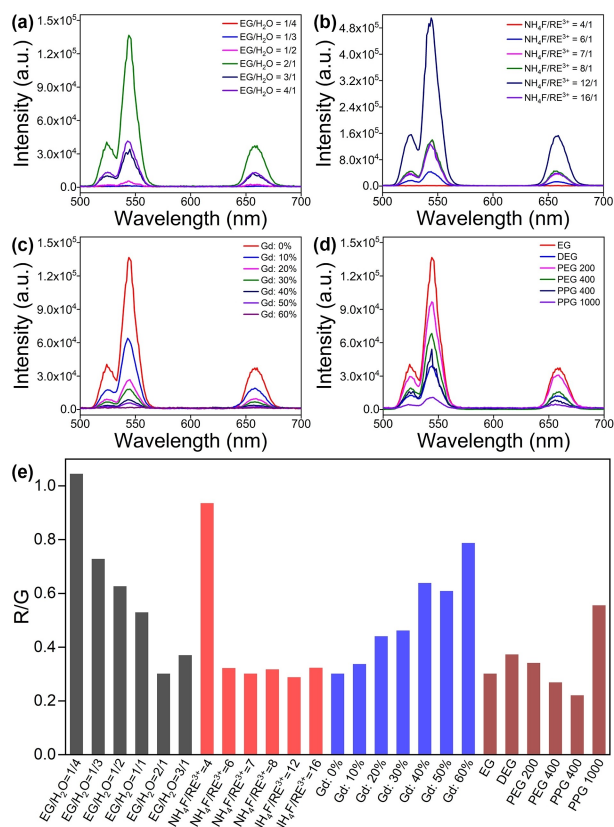


Figure 8. UCL spectra of NaYF₄:Yb/Er prepared under (a) different volume ratios of EG/H₂O, (b) different molar ratios of NH₄F/RE³⁺, (c) different Gd³⁺ dopant ion contents and (d) different organic co-solvents. (e) Corresponding R/G ratio of UC crystals prepared with varying synthetic parameters.

further growth process. The particle size can be controlled by doping with Gd^{3+} ions, while the crystal structure and morphology are independent of activator dopant ions. Interestingly, adding polypropylene glycol the co-solvent apparently favors the formation of microrods with well-defined crystallographic facets.

As to be expected, by appropriately choosing the preparation conditions the upconversion luminescence of these particles, when excited by 976 nm wavelength, can be controlled via their microscopic and mesoscopic structure. Such optimized crystals with adjustable features and unique optical properties may find potential applications in the fields of lighting and display.

Experimental Section

Chemicals

$YCl_3 \cdot 6H_2O$ (99.9%), $YbCl_3 \cdot 6H_2O$ (99.9%), $ErCl_3 \cdot 6H_2O$ (99.9%), $HoCl_3 \cdot 6H_2O$ (99.9%), $TmCl_3$ (99.9%), $GdCl_3$ (99.9%), disodium nitrilotriacetate (DSNTA, 99%), NH_4F (98%), ethylene glycol (EG, 99.9%), diethylene glycol (DEG, 99%), polyethylene glycol 200 (PEG 200), polyethylene glycol 400 (PEG 400), polypropylene glycol 400 (PPG 400), polypropylene glycol 1000 (PPG 1000) were purchased from Sigma-Aldrich. All the chemicals were employed as received without further purification. Milli-Q water (18.2 $M\Omega$ cm at 25 °C) was used in all experiments.

Preparation

In a typical procedure used for the preparation of $NaYF_4:Yb/Er$ (20/2 mol%) crystals, 2 mL of a 0.5 mol/L $RECl_3$ ($RE=Y, Yb$, and Er) solution were added to a solution of 30 mL EG and H_2O (of varying ratio) containing 2 mmol of DSNTA to form metal-ligand complexes (the molar ratio of DSNTA to $RECl_3$ is 2:1). After vigorous stirring at room temperature for 60 min, 7 mmol of NH_4F was added, and the reaction mixture was stirred for another 60 min. Then the reaction mixture was transferred into a 50 mL Teflon bottle held in a stainless-steel autoclave, which was sealed and maintained at 190 °C for 12 h. Afterwards, the autoclave was cooled to room temperature by simply placing it under ambient conditions. The white precipitate was collected by centrifugation and washed once with the ethanol and twice with the water, and then dried in air at 70 °C for 12 h. Other samples, like $NaYF_4:Yb/Ho$ (20/2 mol%) and $NaYF_4:Yb/Tm$ (20/2 mol%) were synthesized in the same manner as described above for the $NaYF_4:Yb/Er$ (20/2 mol%) sample. Additionally, different volume ratios of EG/ H_2O (1/4, 1/3, 1/2, 1/1, 2/1, 3/1), different molar ratios of NH_4F/RE^{3+} (4/1, 6/1, 7/1, 8/1, 12/1, 16/1), different dopant concentrations of Gd^{3+} ion (0~60 mol%) and solvothermal treatment times (2, 4, 6, 12 h) were employed to systematically investigate their impact on the morphological evolution and structural properties of the resulting particles.

Characterizations

Powder X-ray diffraction (XRD) spectra were obtained using Philips X'Pert MPD Pro X-ray diffractometer at a scanning rate of 4°min^{-1} in the 2θ range from 10° to 90° with $Cu K\alpha$ radiation ($\lambda = 0.15406 \text{ nm}$). The energy-dispersive X-ray spectroscopic (EDS) and the morphology analysis were obtained using a field emission scanning electron microscope (FE-SEM, S4000, Hitachi). Transmission electron microscopy (TEM), high-resolution TEM (HR-TEM)

and EDS mapping were performed by FEI Tecnai G2 20 S-TWIN with a LaB6 cathode operating at 200 kV. UC emission spectra were recorded on a calibrated Edinburgh Instruments FSP 920 spectrometer equipped with a 2 W, 976 nm diode laser in Division Biophotonics. The photoluminescence of the crystals was measured with a concentration of 1 mg/mL in ethanol after 10 min ultrasonication, and the measurements were performed at room temperature.

Acknowledgements

Chunning Sun gratefully acknowledges financial support from the China Scholarship Council (CSC, No. 201404910463) and TU Berlin. Michael Schäferling thanks the German Research Council (DFG) for a Heisenberg fellowship. Ute Resch-Genger gratefully acknowledges support by DFG (grant RE1203/20-1, M-Eranet, project NanoHype). We express our gratitude to Steven Orthmann for the XRD and to Christoph Fahrenson for the SEM measurements. Open access funding enabled and organized by Projekt DEAL.

Conflict of Interest

The authors declare no conflict of interest.

Keywords: rare-earth · upconversion · solvothermal · nano-/microcrystals · luminescence

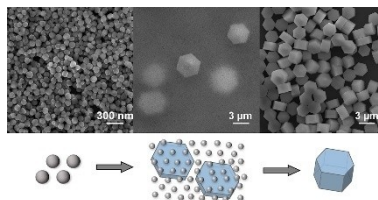
- [1] a) X. Li, F. Zhang, D. Zhao, *Chem. Soc. Rev.* **2015**, *44*, 1346–1378; b) M. Haase, H. Schäfer, *Angew. Chem. Int. Ed.* **2011**, *50*, 5808–5829; *Angew. Chem.* **2011**, *123*, 5928–5950; c) A. Gnach, A. Bednarkiewicz, *Nano Today* **2012**, *7*, 532–563; d) U. Resch-Genger, H. H. Gorris, *Anal. Bioanal. Chem.* **2017**, *409*, 5855–5874.
- [2] a) T. Sabri, P. Pawelek, J. A. Capobianco, *ACS Appl. Mater. Interfaces* **2018**, *10*, 26947–26953; b) M. Guan, H. Dong, J. Ge, D. Chen, L. Sun, S. Li, C. Wang, C. Yan, P. Wang, C. Shu, *NPG Asia Mater.* **2015**, *7*, e205; c) W. Fan, B. Shen, W. Bu, F. Chen, Q. He, K. Zhao, S. Zhang, L. Zhou, W. Peng, Q. Xiao, D. Ni, J. Liu, J. Shi, *Biomaterials* **2014**, *35*, 8992–9002; d) X. Liu, M. Zheng, X. Kong, Y. Zhang, Q. Zeng, Z. Sun, W. J. Buma, H. Zhang, *Chem. Commun.* **2013**, *49*, 3224–3226; e) H. Li, R. Wei, G. Yan, J. Sun, C. Li, H. Wang, L. Shi, J. A. Capobianco, L. Sun, *ACS Appl. Mater. Interfaces* **2018**, *10*, 4910–4920.
- [3] a) X. Zhang, B. Blasiak, A. J. Marenco, S. Trudel, B. Tomanek, F. C. J. M. van Veggel, *Chem. Mater.* **2016**, *28*, 3060–3072; b) F. Vetrone, R. Naccache, A. Juarranz de la Fuente, F. Sanz-Rodríguez, A. Blázquez-Castro, E. M. Rodríguez, D. Jaque, J. G. Sole, J. A. Capobianco, *Nanoscale* **2010**, *2*, 495–498; c) Y.-H. Chien, Y.-L. Chou, S.-W. Wang, S.-T. Hung, M.-C. Liao, Y.-J. Chao, C.-H. Su, C.-S. Yeh, *ACS Nano* **2013**, *7*, 8516–8528; d) Y. Liu, M. Chen, T. Cao, Y. Sun, C. Li, Q. Liu, T. Yang, L. Yao, W. Feng, F. Li, *J. Am. Chem. Soc.* **2013**, *135*, 9869–9876; e) J. Xu, W. Han, T. Jia, S. Dong, H. Bi, D. Yang, F. He, Y. Dai, S. Gai, P. Yang, *Chem. Eng. J.* **2018**, *342*, 446–457.
- [4] a) L. Marciniak, K. Prorok, L. Frances-Soriano, J. Perez-Prieto, A. Bednarkiewicz, *Nanoscale* **2016**, *8*, 5037–5042; b) F. Vetrone, R. Naccache, A. Zamarrón, A. Juarranz de la Fuente, F. Sanz-Rodríguez, L. Martínez-Maestro, E. Martín Rodríguez, D. Jaque, J. García Solé, J. A. Capobianco, *ACS Nano* **2010**, *4*, 3254–3258; c) E. Andresen, U. Resch-Genger, M. Schäferling, *Langmuir* **2019**, *35*, 5093–5113; d) R. J. Meier, J. M. B. Simbürger, T. Soukka, M. Schäferling, *Anal. Chem.* **2014**, *86*, 5535–5540; e) C. Zhang, Y. Yuan, S. Zhang, Y. Wang, Z. Liu, *Angew. Chem. Int. Ed.* **2011**, *50*, 6851–6854; *Angew. Chem.* **2011**, *123*, 6983–6986; f) C. Sun, J. R. J. Simke, M. Gradzielski, *Mater. Adv.* **2020**, *1*, 1602–1607; g) H. Rabie, Y. Zhang, N. Pasquale, M. J. Lagos, P. E. Batson, K.-B. Lee, *Adv. Mater.* **2019**, *31*, 1806991.

- [5] a) X. Chen, W. Xu, H. Song, C. Chen, H. Xia, Y. Zhu, D. Zhou, S. Cui, Q. Dai, J. Zhang, *ACS Appl. Mater. Interfaces* **2016**, *8*, 9071–9079; b) L. Dandan, Y. Shu-Hong, J. Hai-Long, *Adv. Mater.* **2018**, *30*, 1707377; c) M. Tou, Y. Mei, S. Bai, Z. Luo, Y. Zhang, Z. Li, *Nanoscale* **2015**, *8*, 553–562.
- [6] B. Zhou, B. Shi, D. Jin, X. Liu, *Nat. Nanotechnol.* **2015**, *10*, 924–936.
- [7] L. Zong, P. Xu, Y. Ding, K. Zhao, Z. Wang, X. Yan, R. Yu, J. Chen, X. Xing, *Small* **2015**, *11*, 2768–2773.
- [8] R. Martín-Rodríguez, S. Fischer, A. Ivaturi, B. Froehlich, K. W. Krämer, J. C. Goldschmidt, B. S. Richards, A. Meijerink, *Chem. Mater.* **2013**, *25*, 1912–1921.
- [9] Y. Zhu, W. Xu, S. Cui, M. Liu, C. Lu, H. Song, D.-H. Kim, *J. Mater. Chem. C* **2016**, *4*, 331–339.
- [10] P. Li, Y. Zhang, L. Zhang, F. Li, Y. Guo, Y. Li, W. Gao, *Cryst. Growth Des.* **2017**, *17*, 5935–5944.
- [11] F. Wang, X. Xue, X. Liu, *Angew. Chem. Int. Ed.* **2008**, *47*, 906–909; *Angew. Chem.* **2008**, *120*, 920–923.
- [12] H. Qiu, G. Chen, R. Fan, L. Yang, C. Liu, S. Hao, M. J. Sailor, H. gren, C. Yang, P. N. Prasad, *Nanoscale* **2014**, *6*, 753–757.
- [13] a) F. Zhang, Y. Wan, T. Yu, F. Zhang, Y. Shi, S. Xie, Y. Li, L. Xu, B. Tu, D. Zhao, *Angew. Chem. Int. Ed.* **2007**, *46*, 7976–7979; *Angew. Chem.* **2007**, *119*, 8122–8125; b) F. Wang, X. Liu, *J. Am. Chem. Soc.* **2008**, *130*, 5642–5643.
- [14] a) N. J. J. Johnson, A. Korinek, C. Dong, F. C. J. M. van Veggel, *J. Am. Chem. Soc.* **2012**, *134*, 11068–11071; b) J.-C. Boyer, F. Vetrone, L. A. Cuccia, J. A. Capobianco, *J. Am. Chem. Soc.* **2006**, *128*, 7444–7445; c) A. Pilch, C. Würth, M. Kaiser, D. Wawrzyńczyk, M. Kurnatowska, S. Arabasz, K. Prorok, M. Samoć, W. Strek, U. Resch-Genger, A. Bednarkiewicz, *Small* **2017**, *13*, 1701635; d) Y.-W. Zhang, X. Sun, R. Si, L.-P. You, C.-H. Yan, *J. Am. Chem. Soc.* **2005**, *127*, 3260–3261.
- [15] a) R. Luo, T. Li, Y. Chen, Z. Ning, Y. Zhao, M. Liu, X. Lai, C. Zhong, C. Wang, J. Bi, D. Gao, *Cryst. Growth Des.* **2018**, *18*, 6581–6590; b) P. Qiu, R. Sun, G. Gao, B. Chen, C. Zhang, T. Yin, J. Zhang, S. Fang, D. Cui, *ChemNanoMat* **2015**, *1*, 128–134.
- [16] a) Z. Li, Y. Zhang, *Nanotechnology* **2008**, *19*, 345606; b) X. Teng, Y. Zhu, W. Wei, S. Wang, J. Huang, R. Naccache, W. Hu, A. I. Y. Tok, Y. Han, Q. Zhang, Q. Fan, W. Huang, J. A. Capobianco, L. Huang, *J. Am. Chem. Soc.* **2012**, *134*, 8340–8343; c) H. Schäfer, P. Ptacek, H. Eickmeier, M. Haase, *Adv. Funct. Mater.* **2009**, *19*, 3091–3097; d) H. Huang, J. Chen, Y. Liu, J. Lin, S. Wang, F. Huang, D. Chen, *Small* **2020**, *16*, 2000708; e) H. Huang, F. Huang, L. Lin, Z. Feng, Y. Cheng, Y. Wang, D. Chen, *ACS Appl. Mater. Interfaces* **2019**, *11*, 46379–46385.
- [17] X. Wang, J. Zhuang, Q. Peng, Y. Li, *Nature* **2005**, *437*, 121–124.
- [18] F. Wang, Y. Han, C. S. Lim, Y. Lu, J. Wang, J. Xu, H. Chen, C. Zhang, M. Hong, X. Liu, *Nature* **2010**, *463*, 1061–1065.
- [19] a) F. Wang, D. K. Chatterjee, Z. Li, Y. Zhang, X. Fan, M. Wang, *Nanotechnology* **2006**, *17*, 5786; b) D. K. Chatterjee, A. J. Rufaihah, Y. Zhang, *Biomaterials* **2008**, *29*, 937–943.
- [20] Z. Li, Y. Zhang, *Angew. Chem. Int. Ed.* **2006**, *45*, 7732–7735; *Angew. Chem.* **2006**, *118*, 7896–7899.
- [21] a) C. Li, Z. Quan, J. Yang, P. Yang, J. Lin, *Inorg. Chem.* **2007**, *46*, 6329–6337; b) C. Li, C. Zhang, Z. Hou, L. Wang, Z. Quan, H. Lian, J. Lin, *J. Phys. Chem. C* **2009**, *113*, 2332–2339; c) C. Li, J. Yang, Z. Quan, P. Yang, D. Kong, J. Lin, *Chem. Mater.* **2007**, *19*, 4933–4942; d) C. Li, Z. Quan, P. Yang, S. Huang, H. Lian, J. Lin, *J. Phys. Chem. C* **2008**, *112*, 13395–13404.
- [22] F. He, N. Niu, L. Wang, J. Xu, Y. Wang, G. Yang, S. Gai, P. Yang, *Dalton Trans.* **2013**, *42*, 10019–10028.
- [23] J. Yang, D. Shen, X. Li, W. Li, Y. Fang, Y. Wei, C. Yao, B. Tu, F. Zhang, D. Zhao, *Chem. Eur. J.* **2012**, *18*, 13642–13650.
- [24] a) C. Li, X. Yin, L. Chen, Q. Li, T. Wang, *Chem. Eur. J.* **2010**, *16*, 5215–5221; b) G. Wang, X. Gou, J. Horvat, J. Park, *J. Phys. Chem. C* **2008**, *112*, 15220–15225; c) C. An, G. Liu, Y. Wang, L. Li, F. Qiu, Y. Xu, C. Xu, Y. Wang, L. Jiao, H. Yuan, *RSC Adv.* **2013**, *3*, 15382–15388.
- [25] Y. Song, H. You, Y. Huang, M. Yang, Y. Zheng, L. Zhang, N. Guo, *Inorg. Chem.* **2010**, *49*, 11499–11504.
- [26] M. Ding, C. Lu, L. Cao, Y. Ni, Z. Xu, *CrystEngComm* **2013**, *15*, 8366–8373.
- [27] J. A. Damasco, G. Chen, W. Shao, H. Ågren, H. Huang, W. Song, J. F. Lovell, P. N. Prasad, *ACS Appl. Mater. Interfaces* **2014**, *6*, 13884–13893.
- [28] G. Ajithkumar, B. Yoo, D. E. Goral, P. J. Hornsby, A.-L. Lin, U. Ladiwala, V. P. Dravid, D. K. Sardar, *J. Mater. Chem. B* **2013**, *1*, 1561–1572.
- [29] M. Kraft, C. Würth, V. Muhr, T. Hirsch, U. Resch-Genger, *Nano Res.* **2018**, *11*, 6360–6374.
- [30] F. Auzel, *Chem. Rev.* **2004**, *104*, 139–174.
- [31] J. Zhou, Q. Liu, W. Feng, Y. Sun, F. Li, *Chem. Rev.* **2015**, *115*, 395–465.
- [32] S. Wilhelm, M. Kaiser, C. Wuerth, J. Heiland, C. Carrillo-Carrion, V. Muhr, O. S. Wolfbeis, W. J. Parak, U. Resch-Genger, T. Hirsch, *Nanoscale* **2015**, *7*, 1403–1410.
- [33] G. S. Yi, G. M. Chow, *Adv. Funct. Mater.* **2006**, *16*, 2324–2329.

Manuscript received: October 23, 2020
 Revised manuscript received: December 8, 2020
 Accepted manuscript online: December 10, 2020
 Version of record online: December 28, 2020

FULL PAPER

The evolution of lanthanide-doped NaYF₄ upconversion crystals under solvothermal conditions is reported.



*C. Sun**, Prof. Dr. M. Schäferling, Dr. U. Resch-Genger, Prof. Dr. M. Gradzielski*

1 – 11

Solvothermal Synthesis of Lanthanide-doped NaYF₄ Upconversion Crystals with Size and Shape Control: Particle Properties and Growth Mechanism

